Ultrasonics 95 (2019) 13–21

Contents lists available at ScienceDirect

Ultrasonics

journal homepage: www.elsevier.com/locate/ultras

Ultrasonic non-destructive testing of complex titanium/carbon fibre composite joints

Elena Jasiūnienė[a,*], Liudas Mažeika[a], Vykintas Samaitis[a], Vaidotas Cicėnas[a], David Mattsson[b]

[a] Ultrasound Institute, Kaunas University of Technology, Kaunas, Lithuania
[b] Swerea SICOMP AB, Pitea, Sweden

ARTICLE INFO

Keywords:
Hybrid joints
Adhesive bonding
Non-destructive testing
Ultrasonic testing

ABSTRACT

Ultrasonic inspection is widely used for non-destructive evaluation of composite adhesive joints. However, there are serious challenges in applying ultrasonic testing on metal to composite hybrid joints, because they are multi-layered, made out of dissimilar materials and relatively thin. The ultrasonic signals reflected by different layers are overlapped, scattered and attenuated. The aim of this research was to develop an ultrasonic inspection technique suitable for defect detection in hybrid metal to composite joints where the metal part has pin arrays, which entangle with the composite part. The immersion pulse echo technique was used to collect data. In order to overcome the problems related to the rough surface and non-parallel layers a novel signal post-processing algorithm for reconstruction of the joint area was developed and validated experimentally. It is shown that using the proposed technique the positions of different defects can be determined.

1. Introduction

The transport sector has been increasingly growing in the past few decades. This leads to huge emissions of carbon dioxide (CO_2) and other greenhouse gasses that continually drive the global warming and ocean acidification. To reduce the carbon dioxide emissions, the concept of lighter hybrid structures has been introduced which is based on combining two or more lightweight materials, such as metals and composites. However, hybrid structures made of dissimilar materials can only be reliable if their joint is effective. Since the joined materials possess mechanical property mismatch, different surface chemistry and temperature behaviour, many challenges have to be solved in order to produce reliable and high strength joints.

There are many existing methods for joining dissimilar materials, e.g. mechanical fastening or adhesive bonding. The mechanical fastening, i.e. bolted joints or riveting requires drilling, which damages the fibres of the composite and creates a potential weak spot in the structure. A huge attention has been paid by the researchers to improve the quality of the mechanical joints, analysing the relations between the stress-strain and the joint geometry [1,2], bolt diameter [3], bolt torque tightening hole clearance [4–6], washer size [7], rivet features [8] etc. However, since the joining process involves the use of composites, the adhesive bonding is often used as an alternative. Such approach is non-invasive, even more lightweight and provides uniform distribution of stresses across the joint. On the other hand, adhesive bonds are vulnerable to delaminations, voids and zero volume disbond type defects that create a weak bond spots having the tendency to develop. Thus such joints possess relatively low adhesion strength and require larger bonding areas, good surface preparation and pre-treatment like etching [9–14]. Moreover, the adhesives itself tend to degrade over time; hence, the failure can be very sudden and unexpected [15].

Recently the concept of the hybrid joints was introduced in which the adhesive bonds are strengthened with metal/fibre inserts or bolts, combining the advantages of both mechanical fastening and adhesive bonding [16–18]. A comprehensive study related to hybrid bolted/bonded joints was presented by Marannano et al. [19] and Di Franco et al. [20], who analysed mechanical performance of these joints to highlight their advantages over regular adhesively bonded and simply bolted joints. Lately, a great amount of attention was paid on the hybrid joining techniques that are based on special metal pin arrays, which provide mechanical interlocking between bonded materials. In contrast to bolted/bonded joints, such pinning technology minimizes the damage to the composite fibres and improves mechanical properties of the joint. The mechanical properties of such joints depend mainly on three major factors: the technology, which is used to build or insert the pins; volume, diameter of the pins; and the quality of the adhesion [21,22]. In case of composite-composite joint, the special z-pins are inserted as reinforcements in the uncured prepreg stack using the ultrasonically

* Corresponding author.
E-mail address: elena.jasiuniene@ktu.lt (E. Jasiūnienė).

https://doi.org/10.1016/j.ultras.2019.02.009
Received 11 December 2017; Received in revised form 6 February 2019; Accepted 24 February 2019
Available online 28 February 2019
0041-624X/

assisted z-fibre UAZ technique [23–25]. Since the technology uses carrier foam and ultrasonic horn to insert the z-pins, it is vulnerable to inaccurate insertion, which may swell the laminate and reduce the mechanical performance of the joint. Meanwhile, for the metal composite joints, the pins are being built on the metal part mostly using either surface treatment ST [10], additive manufacturing AM [26] or cold metal transfer CMT [27,28]. Due to the manufacturing technique, the ST and CMT are usually limited to some certain pin geometries only [10,29]. The additive manufacturing (AM) is one of the most attractive among them, since it ensures low scrap rate and freedom of designing complex geometries without the need for expensive tools or fixtures. It is based on successive melting of thin layers of metal powder, hence the structure is being built layer after layer. There are many existing studies focusing on the static, fatigue and environmental performances of differently produced pinned composite-composite or metal-composite joints [30–37].

Usually in the production of the metal-composite hybrid joints, the metal pins are inserted into a dry composite fabric, followed by insertion of the resin using vacuum infusion. During the curing process, various defects such as cracks, debonding and delaminations can occur especially in the areas around the pins, between the layers of composite or at the metal-composite interface. The presence of any defects during the manufacturing process may weaken the bond integrity and overall performance of the entire joint. Most of the defects in the joints occur due to insufficient amount or uneven application of the adhesive, inclusion of foreign materials, contamination, poor surface preparation and fibre swelling [38]. The quality of the joint is usually determined using destructive mechanical tests [39–41]. However, mechanical testing can be used only under the development stage of the joining technique. For the quality control of manufacturing processes or periodic inspection of in-service joints, non-destructive testing techniques must be used.

Ultrasonic measurement techniques have been widely used for non-destructive evaluation of regular adhesive joints. Different approaches to detect the disbond defects, delaminations or degradation of adhesive has been proposed by many authors including application of resistance measurements [42], shear [43], longitudinal [44–48], guided waves [49–56] and non-linear ultrasonic testing (UT) [57,58]. The above-mentioned authors demonstrated some different approaches for quality control of adhesive joints. For example, Ramadas et al. [54] analysed propagation of fundamental A0 mode on the wind turbine blade sample. The authors found that the A0 mode converts to symmetrical S0 mode at the presence of the spar web and the “turning modes” are being generated which propagate back and forth at the T-joint. Kumar et al. [43] suggested that the reflection amplitude of shear waves from adhesive layer might be used as an indicator to detect interface degradation. Titov et al. [44] proposed to defect disbond defects by measuring reflection coefficient and phase inversion of longitudinal waves. The main challenges in UT of joints reported by these authors were related to non-parallel surfaces, significant reverberations in metal part that can mask the other echoes, overlapping reflections due to thin layers, scattering and attenuation in composite part. The introduction of the hybrid joints with pin arrays make the UT even more challenging due to small, conically headed pins and manufacturing technology, which produces rough surfaces to improve the adhesion. The major concern in quality assessment of adhesive joints is detection of zero volume interfacial disbonds, also known as kissing bonds [14]. Such type of defects are complicated to detect by conventional ultrasonic techniques, as two surfaces are either partially bonded or touching with no forces, which makes them transparent to ultrasonic waves, while providing a weak bond strength [59]. Such defects are usually detected using non-linear ultrasonic techniques as dynamic vibration of the structure causes non-linear oscillation of the defect and different sub and super harmonics appear in the output signals [60,61]. Meanwhile this research focuses on the inspection of hybrid joints, where the main defect types are delaminations and disbonds that appear during the production, especially in the areas around pins.

Despite numerous literature studies on structural assessment of regular adhesive joints, a little attention has been paid to NDE of hybrid joints made from dissimilar (metal and composite) materials. Recently, Parkes et al. [29] reported some approaches on ultrasonic C-scan inspection of CFRP-Titanium joints to determine strength of the adhesion at different load levels. The authors suggested performing the inspection from the metal side of the sample as the laminate structure and the pins scatter the incident signal. Such approach can be effectively used to detect broken pins by monitoring the time of flight of the signal reflecting back from the joint interface and the tip of the pin. Alternatively, it can be used to detect disbond between the interface of metal and composite, as the reflection amplitude in case of defect is expected to be stronger than those from good bond. However, this approach cannot be applied to detect the delaminations between the layers of the composite and around the pins, which can be significant cause of the joint failure as well. The microstructure analysis of various pinned joints demonstrated that due to the presence of pins, the laminate fibres are pushed aside and bent, hence the laminate waviness occur [62,63]. The volume of wavy fibres increases rapidly with the increase of the number of pins and their diameter [33]. The ply waviness around pins can act as the initiating point of delamination type defects, which may lead to further joint failure. The mechanical tests have confirmed that the failure in the joint usually occurs due to rapid delamination crack growth, which leads to complete detachment of composite [64,65]. Therefore, some techniques suitable to inspect both the composite part of the joint and the adhesion layer should be developed accordingly.

The aim of this research was to develop an ultrasonic NDT technique, suitable for detection of defects in hybrid metal-composite joints. Samples of an innovative titanium/carbon fibre composite joint with artificial and natural defects have been studied using high frequency focused transducers. A special ultrasonic signal post-processing method for reconstruction of the joint area and detection of defects inside the composite has been proposed and tested with the experimental data. It was demonstrated that the proposed ultrasonic NDT technique allows reconstructing the complicated structure of the interface between the metal and composite, even when the measurements are performed from the CFRP side, which introduces an additional noise. Using the proposed method, the positions and approximate depths of the artificial defects were determined.

2. Fabrication of the dissimilar joint sample with defects

The additive manufacturing technology was used to build an adherent with pin array. In this study, Ti6AIV grade titanium was selected. The titanium part was free formed from powder using a melting technique implementing an electron beam in vacuum. As a result, a material with excellent properties, with low impurities and low residual stress is obtained. A photo of the titanium adherent is presented in Fig. 1a. The composite part was manufactured using a carbon non-crimp fabric (NCF) weave (HTS45 filament yarn), where 16 layers in total were stacked together on the titanium part before infusion of the resin in the form of Araldite LY556. Hence, the joint consists of a free formed titanium adherent and a CFRP part. The cross-section of the investigated structure is presented in Fig. 1b.

Fig. 2a shows a schematic top view picture of the arrangement of the pin array of the titanium adherent. Five missing pins in different positions can be observed. Also a release film inserts in the form of a 7.5 μm Upilex® polyimide were used to create the artificial delaminations in the joint sample (one in the zone without pins, one in the zone with pins). Bottom view of the sample is shown in Fig. 2b, top view of the sample – in Fig. 2c.

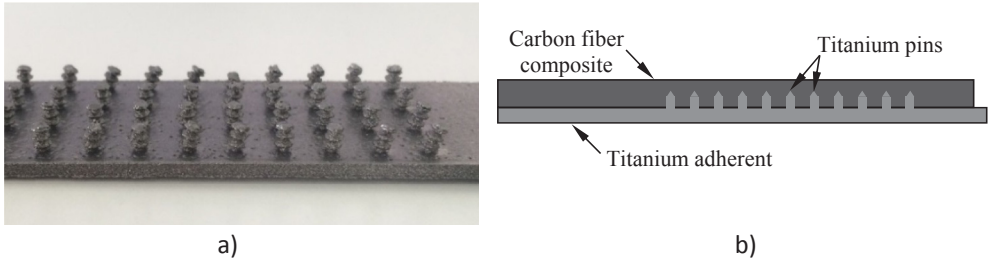

Fig. 1. An adherent with a pin array produced from the titanium powder (a) and the schematic diagram of a hybrid joint (b).

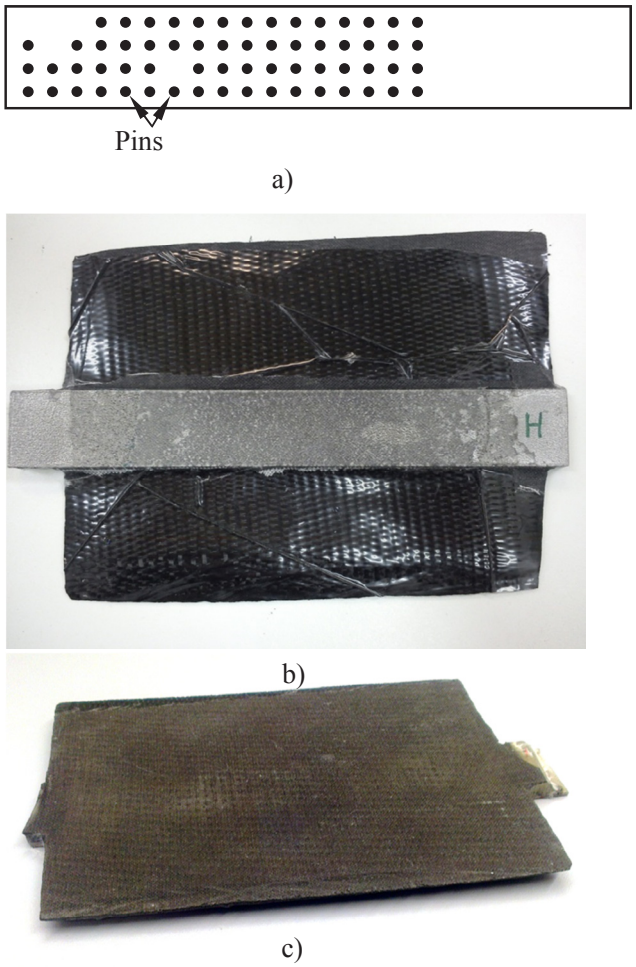

Fig. 2. A schematic top view picture of the location of the release films in the joint (a), bottom view of the sample (b), top view of the sample (c).

3. Quality assessment of the prefabricated titanium-composite joint

The objective of the non-destructive testing is to detect both broken/missing pins and the artificially introduced delaminations. The complicated geometry (pins) and inhomogeneous structure (anisotropic microstructure of titanium and CFRP composite) of the prefabricated joints makes non-destructive inspection challenging. Thus, the proper inspection technique has to be selected first. The immersion pulse echo technique is the most common method to inspect the adhesive joints [13]. However, in the case of dissimilar joints, success of pulse-echo technique is dependent on the orientation of sample according to the transducer, i.e. if the testing is performed from the metal or from the composite side.

3.1. Inspection set-up alternatives

The first step in selection of the suitable inspection set-up and orientation of the sample was to evaluate the expected amplitudes of the signals reflected by the surface and interfaces of the hybrid joint in case of the inspection from the titanium and from CFRP side. Two separate estimations were performed, one for the healthy hybrid joint and another one for the joint with an air gap as delamination type defect. For this evaluation, only the acoustic impedance differences of the layered structure were taken into account. The reflection coefficient was calculated according to the equation:

$$R = \frac{Z_2 - Z_1}{Z_2 + Z_1}, \tag{3.1}$$

where Z_1 – is the acoustic impedance of the first medium, Z_2 – is the acoustic impedance of the second medium, $Z = \rho \cdot c$, (where ρ – is the density of the propagating medium, c – is the velocity of longitudinal ultrasonic waves in that particular medium).

The theoretical estimation of the reflection coefficients was performed in four separate cases (Fig. 3):

a) inspection from the CFRP side – good joint (Fig. 3a);
b) inspection from the CFRP side – joint with delamination (Fig. 3b);
c) inspection from the titanium side – good joint (Fig. 3c);
d) inspection from the titanium side – joint with delamination (Fig. 3d).

The estimated reflected amplitude values are summarized in Fig. 3 and Table 1.

The results demonstrate that in the case of inspection from the CFRP side the normalized amplitude of the signal reflected from the surface is 0.28, while in the case of inspection from the Ti side the normalized amplitude of the same reflection is 0.805 (see Table 1). It means, that the signal, which reaches the interface to be inspected (CFRP-Ti) is much stronger in the case of the inspection from the CFRP side. Furthermore, if to look at the amplitude values at the interface between the CFRP and Ti, amplitude of the signal reflected from the interface is 0.255 in the case of inspection from the CFRP side compared to 0.019 in the case of the inspection from the Ti side.

The task of the NDT is to evaluate the quality of the interface, i.e. it has to be differentiated, if the quality of the joint is good, or is there a disbond between layers. It means that from the signal reflected from the interface, evaluation of the quality of the joint has to be made. In the case of the inspection from the CFRP side difference in signal amplitude of a good joint/bad joint is 0.255/0.520, while in case of the inspection from the Ti side 0.019/0.038. In both cases, difference is approximately twice, but in the case of the inspection from the Ti side amplitude of the informative signal (reflected from the interface) will be approximately 13 times smaller than in the case of the inspection from CFRP side. Calculations show, that scanning from the CFRP side can assure much stronger amplitude of the signal reflected from the dissimilar interface and also bigger difference in reflected amplitudes of a good joint and a bad joint.

However, there are drawbacks of scanning from the CFRP side as

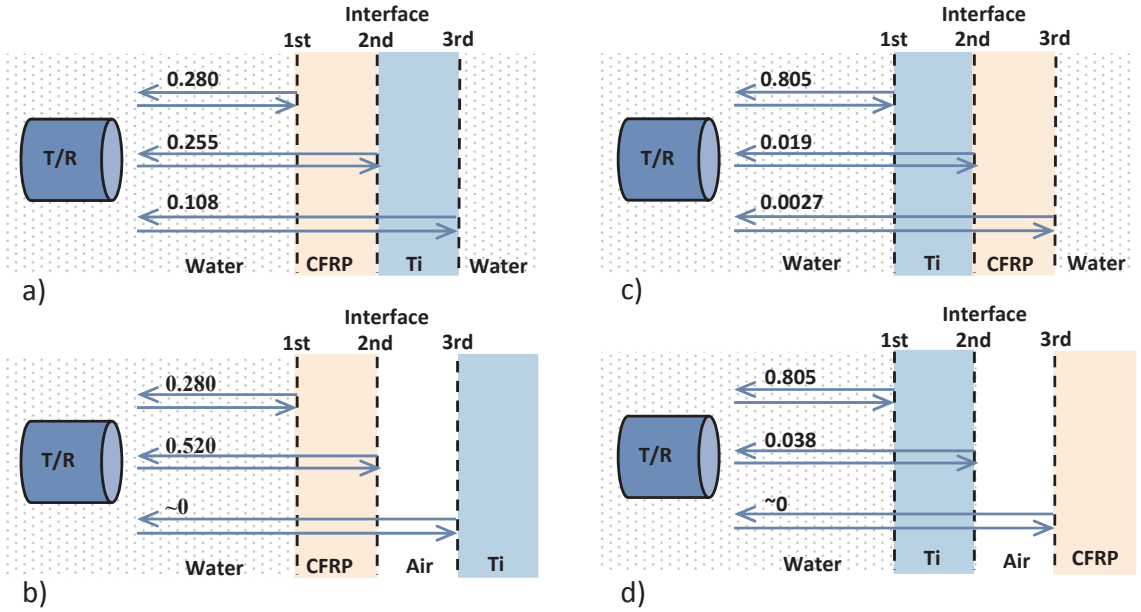

Fig. 3. Calculated normalized amplitude values of the received signal for different inspection set-ups: (a) inspection from the CFRP side – good joint, (b) inspection from the CFRP side – joint with delamination, (c) inspection from the titanium side – good joint, (d) inspection from the titanium side – joint with delamination.

Table 1
Calculated normalized amplitude values at the surface of ultrasonic transducer.

Layered structure*		Reflected normalized amplitude from		
		1st interface	2nd interface	3rd interface
a.	W → CFRP → Ti → W	0.280	0.255	0.108
b.	W → CFRP → Air → Ti	0.280	0.520	~0
c.	W → Ti → CFRP → W	0.805	0.019	0.0027
d.	W → Ti → Air → CFRP	0.805	0.038	~0

* W – water, Ti – titanium, CFRP – carbon fibber reinforced plastic, Air – delamination defect as an air layer.

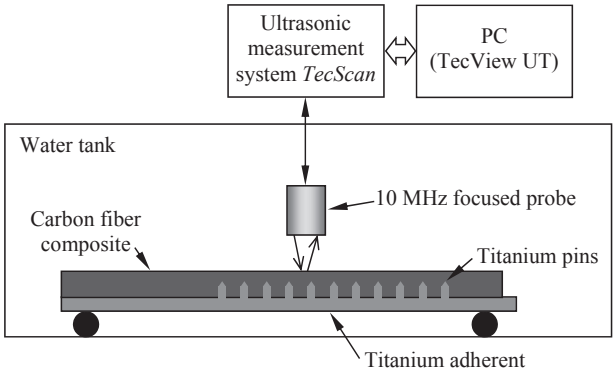

Fig. 4. The experimental set-up for quality assessment of hybrid joint.

well: surface of the CFRP layer is rough and not parallel to the interface with the titanium, thickness of the CFRP layer can vary and therefore it is not possible to predict the exact arrival time of the signal reflected from the interface. Additionally, the CFRP layer has non-homogenous structure. Therefore, in B-scan image signal reflected by the interface will appear not in constant time window. Its position in time domain will vary depending on the thickness of composite layer. Nevertheless, as was shown above, scanning from the CFRP side can assure much stronger amplitude of the signal reflected from the dissimilar interface. In addition, the informative signal will not be overlapped by multiple reflections as in case of inspection from titanium side. In addition, the measurement from the CFRP side can detect not only the delamination in dissimilar joint, but the defects within the CFRP layer as well. The investigations of Milne et al. [66] show, that the sensitivity of pulse echo technique in titanium is limited also due to noise backscattered by the anisotropic microstructure of titanium.

The main reason why inspections of such structures are performed from titanium side is related to the complicated prediction of the arrival time of signal reflected from the interface because of variation of CFRP layer thickness [13]. This problem can be solved by the development of special signal processing algorithm for detection of dissimilar interface.

3.2. Experimental investigations and set-up

To test the performance of the proposed signal processing technique, the experiments have been carried out on the prefabricated hybrid joint with artificial delaminations. The sample with hybrid joint was immersed into the water tank, facing the composite part up as it is shown on Fig. 4. The pulse-echo data of the sample was acquired by scanning the 10 MHz focused transducer across the entire surface with the spatial resolution of 0.5 mm. The spacing between the sample and the transducer was selected to get focal point approximately at the composite-metal interface. The transducer was driven with 50 V spike pulse. At the reception side, the waveforms were recorded using 200 MHz sampling frequency. At each position, the reflected signals were measured 64 times and averaged to ensure better signal to noise ratio. The experimental set-up for data acquisition is presented in Fig. 4.

3.3. Signal processing algorithm

In the case of dissimilar joints, properties of joined materials (acoustic impedances) are different, meaning that the signal from the joint will be reflected even without defects in it. Hence, the detection of defects in dissimilar joints is challenging task for conventional ultrasonic techniques. In addition, the rough surface and non-planar interface presents additional challenge to be solved. However, the main problem of the measurement data analysis in the case of dissimilar joints is the presence of non-parallel structures with varying thickness. This leads to the fact that delay time of the signals reflected from the surface and from the interface of the sample is varying during the scan. Conventional techniques based on moving time window using same

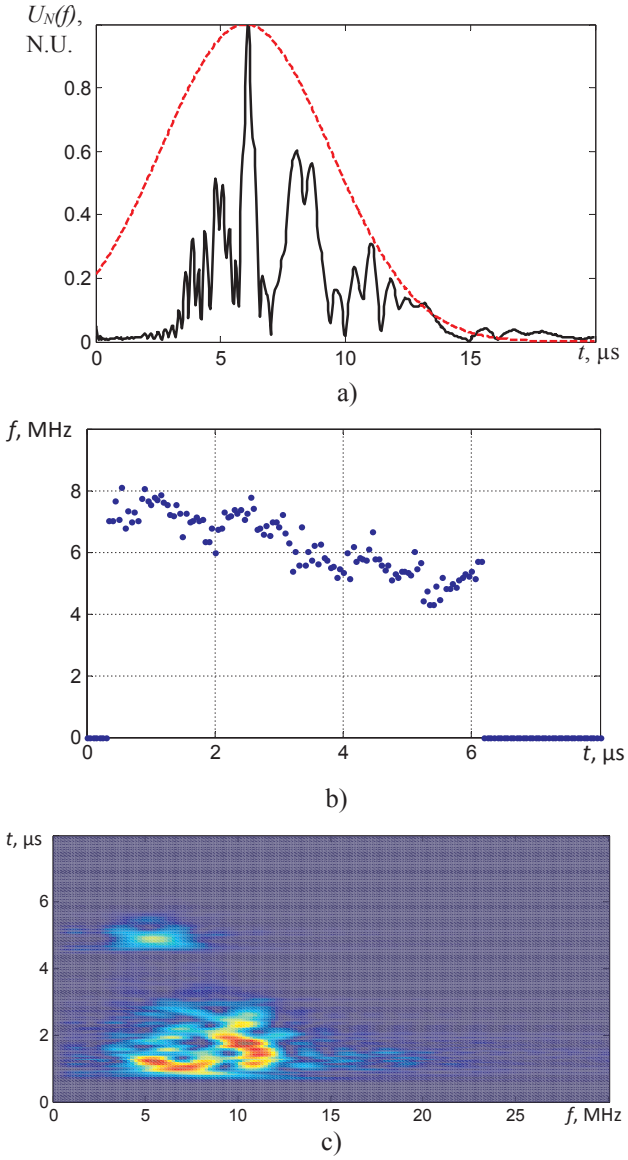

Fig. 5. Analysis of the reflected signals, a –spectrum of the signal reflected by interface, b – mean frequency of the spectrum, c – 2D frequency spectrum of the B-scan.

threshold level do not work due to high variation of signal amplitude caused by scattering effects in the structure. In order to overcome this problem, the novel processing algorithm has been developed. It enables to detect the interface between two material layers and then "equalize" it. The signal processing is performed separately on each B-scan data according to the algorithm presented below:

1. Each signal is filtered using Gaussian filter in order to reduce the structural noise:

$$u_F(t) = \mathrm{Re}\{\mathrm{FT}^{-1}[U(f)\cdot H_G(f)]\}, \tag{3.2}$$

where $(f) = FT[u(t)]$; $u(t)$ is the measured signal; $H_G(f) = e^{-\frac{ln2}{\Delta f_F}\cdot(f-f_{0F})^2}$ is the Gaussian filter; f_{0F} is a central frequency and $\Delta f_F$is a bandwidth at 6 dB level.

2. Mean frequency of the spectrum of the signals along the sample versus time was calculated as follows

$$\bar{f}([t_k : t_k + \Delta t_w]) = \frac{1}{N_{Bsc}} \sum_{k_{Bsc}=1}^{N_{Bsc}} f_{k_{Bsc}}([t_k : t_k + \Delta t_w]) \tag{3.3}$$

$$\text{where } f_{k_{Bsc}}([t_k : t_{k-1}]) = \frac{\sum_{k_f=1}^{N_{kf}} f_{k_f}\cdot U_k(f_{k_f})}{\sum_{k_f=1}^{N_{kf}} U_k(f_{k_f})} \tag{3.4}$$

$$U_k(f) = FT\{u([t_k : t_k + \Delta t_w])\} \tag{3.5}$$

$$f_{k_f} \in [U_k(f = f_{k_f}) > U_{\mathrm{th}}] \tag{3.6}$$

$$t_k = (k-1)\cdot dt_w,\ k = 1{:}\ N_k \tag{3.7}$$

dt_w is the step of time window shift, Δt_w is the width of time window, N_k is the total number of time window positions, N_{Bsc} is the number of the signals in the B-scan under analysis, U_{th} – is the threshold level for spectrum analysis.

3. The arrival time of the signal reflected by the interface is estimated. For that purpose, each signal in B-scan is analysed in following order:

- The time interval in which the interface reflection can be expected is defined by:

$$u_w(t) = u_F(t)\cdot h_{\mathrm{RW}}(t,\ t_{0W},\ T_W) \tag{3.8}$$

where $h_{\mathrm{RW}}(t,\ t_{0W},\ T_W)$ is the rectangular time window function; t_{0W}, T_W is the start instance and duration of the time window respectively.

- The maximum of the windowed signal is calculated: $U_{\max} = \max[u_w(t)]$.
- The time instance at which the signal exceeds −6dB level with respect to the signal maximum is estimated:

$$t_{6\mathrm{dB}} = min(t_k),\ u_w(t_k) > 0.5U_{\max} \tag{3.9}$$

- The analysis is continued only in the case if:

$$\max\{|u_w(t_k)|\} < 0.5U_{\max},\ \text{for}\ \ t_{0W} \le t_k \le t_{0W} + T_0 \tag{3.10}$$

where $T_0 = 1/f_0$, f_0 is the central frequency of the transducer. If Eq. (3.10) is valid, the zero crossing instance t_{zc} in the signal such that $t_{zc} < t_{6\mathrm{dB}}$ is estimated using third order polynomial approximation. If the Eq. (3.10) is not valid, it means that the interface reflection is completely hidden in structural noise, arrival time cannot be estimated and t_{zc} is assigned to be zero ($t_{zc} = 0$).

As the result of this step the set of the arrival times of interface reflections $t_{zc}(x_k)$ along B-scan is obtained, where x_k, $k = 1\tilde{A}\cdot K$ are positions along x axis at which the signals were recorded, K is the total number of positions.

4. The dependency $t_{zc}(x_k)$ obtained in previous step is not continuous, at some positions it contains zeros (not estimated values) or some sharp spikes caused by uncertainties related to structural noise or roughness of the surface. The arrival time at these positions is obtained using linear interpolation between two "correct" neighbour values. The "correct" values are assumed to be at such positions x_k^c, which satisfy equation:

$$\left|\frac{t_{zc}(x_k^c)}{dx_k}\right| \le L_c \tag{3.11}$$

where L_c is threshold level. As a result, the corrected dependency of arrival time of the signal reflected by the interface $t_{zc}^c(x_k)$ is obtained.

5. The B-scan aligned with respect to interface is obtained by shifting each of the signals in the time domain according to estimated arrival time:

$$u_{sh}(t,\ x_k) = u(t - t_{zc}^c(x_k) + t_{0W},\ x_k) \tag{3.12}$$

6. In order to reduce the structural noise in the front of the interface, reflected signals are filtered using Gaussian time domain filter:

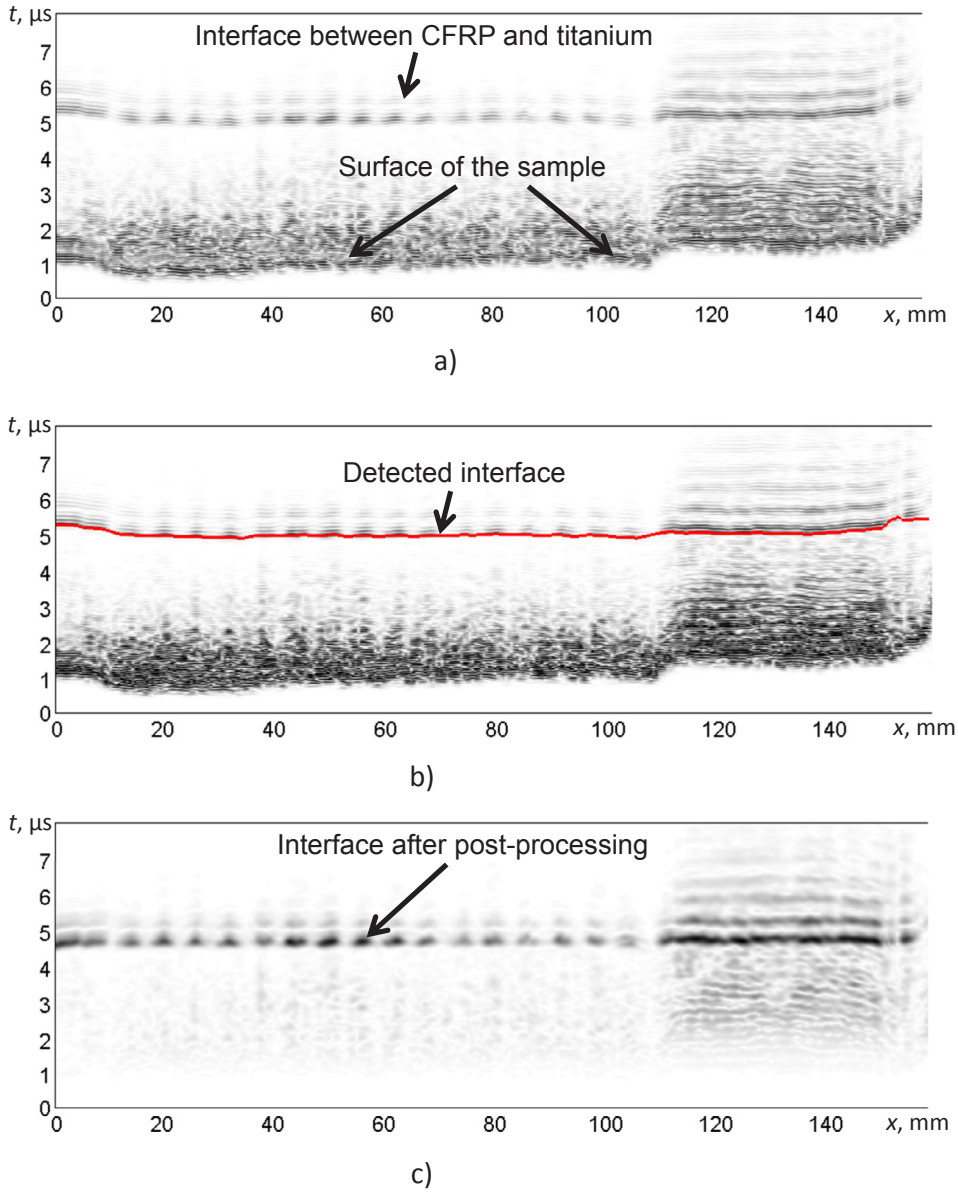

Fig. 6. Raw B-scan image obtained on the CFRP-titanium sample with pins (a), detected interface between the CFRP and titanium using the proposed post-processing algorithm (b), the interface after the post processing (c).

$$u_{sh}^{F}(t, x_k) = u_{sh}(t, x_k) \cdot h_{str}(t) \tag{3.13}$$

where $h_{str}(t) = \begin{cases} e^{-K_{str}\left(\frac{t_{0W}-t}{t_{0W}}\right)^2} & t \le t_{0W}, \\ 1 & t > t_{0W}, \end{cases}$

and K_{str} is the coefficient defining steepness of the filter, in our case $K_{str} = 0.2$.

7. The envelope of each signal in B-scan is calculated:

$$u_{sh}^{\mathrm{FH}}(t, x_k) = hilbert\,[u_{sh}^{F}(t, x_k)] \tag{3.14}$$

8. The data for 3D imaging are prepared by calculating maximum value for each signal:

$$u_{3\mathrm{D}}(t_n, x_k) = \max_{t}\,[u_{sh}^{\mathrm{FH}}(t, x_k)],\ t \ni [(n-1)\cdot\Delta t_{3\mathrm{D}} \div n\cdot\Delta t_{3\mathrm{D}}] \tag{3.15}$$

where $\Delta t_{3\mathrm{D}}$ is sampling step in time domain selected for 3D imaging.

4. Results and discussion

To test the performance of the proposed signal processing technique, the experiments have been carried out on the prefabricated hybrid joint sample with artificial defects – missing pins and delamination type defects. The sample with hybrid joint was immersed into the water tank; measurements from both titanium and composite side were performed to verify the theoretical considerations in part 3.1 (inspection set-up alternatives). Experimental measurements proved that non-destructive testing from the titanium side is impossible. So setup with transducer facing the composite part up as it is shown on Fig. 4 was selected for further investigations.

Time frequency analysis of the reflected signals have shown that the part of the signal corresponding to the interface reflection possess lower frequency bandwidth compared to the surface reflection as the higher frequencies are more affected by scattering and attenuation (Fig. 5a). It can be observed from the presented figure that even though the 10 MHz signal was transmitted, central frequency of the reflected signal is 6 MHz

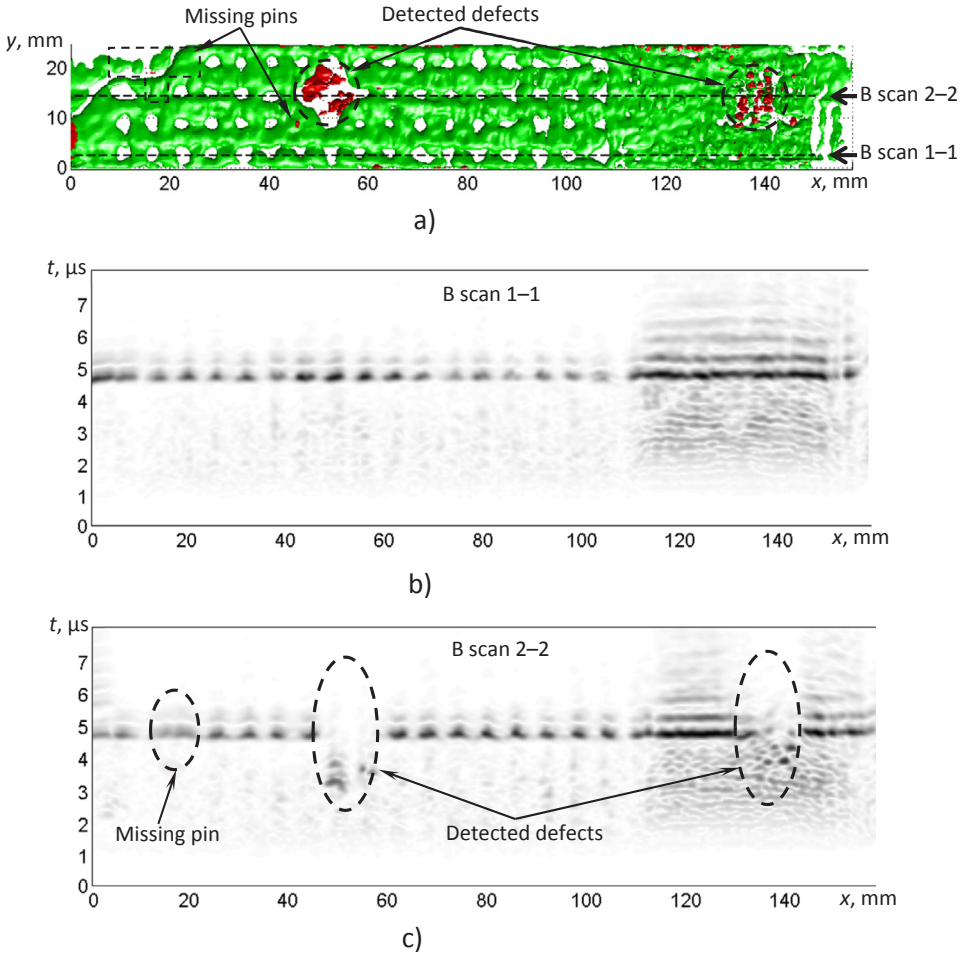

Fig. 7. The C-scan of the reconstructed interface between the CFRP and titanium in 3D (green) and the defect positions (red) (a), B-scan at 1st position (b), B-scan at 2nd position (c). (For interpretation of the references to colour in this figure legend, the reader is referred to the web version of this article.)

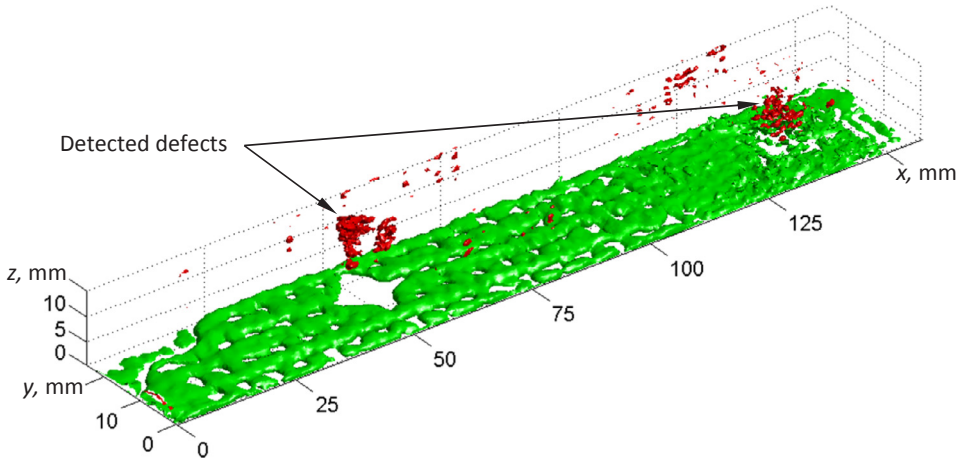

Fig. 8. The 3D C-scan of the reconstructed interface between the CFRP and titanium in 3D (green) and the defect positions (red). (For interpretation of the references to colour in this figure legend, the reader is referred to the web version of this article.)

Mean frequency of the spectrum of the signals (Eq. (3.3)) along the sample was analysed and is presented in Fig. 5b. It can be observed as well, that the frequency of the signal decreases going deeper into the sample. 2D frequency spectrum of B-scan, presented in Fig. 5c, also proves this observation – reflection from interface (at 4,5 µs) possesses lower frequencies than the surface reflection.

So, in order to increase the amplitude of the interface reflection compared to the surface reflection, the central frequency of the filter was selected slightly lower compared to the frequency of transducer. After investigating multiple cases, it was determined, that the width of the filter should be close to the bandwidth of the transducer.

In Fig. 6 B-scan images obtained on the CFRP-titanium sample with pins are presented before and after post processing: raw B-scan image (a), detected interface between the CFRP and titanium using the proposed post-processing algorithm (b) and the interface after the arrival time correction (c). It can be observed that special post processing

method enabled to detect interface between two materials (Fig. 6b) and then to “eqlize” it (Fig. 6c), i.e. to eliminate the influence of not flat surface of the sample.

In Fig. 7a the C-scan of the reconstructed interface between the CFRP and titanium in 3D (green) and the defect positions (red) are presented. Two delamination type defects (coloured in red) can be observed, as well as the positions of all five missing pins can be indicated. In Fig. 7b B-scan 1–1 is presented, in Fig. 7c B-scan 2–2 is presented. Analysing B-scan 1–1 (Fig. 7b) it can be observed, that no defects are present at this slice, and homogeneous pattern indicates that all pins are present, and zone with no pins on the right part of the sample could be indicated as well. In B-scan 2–2, (Fig. 7c) indications of two delamination defects are visible, as well as one missing pin. Analysing B-scan it can be observed, that the delamination defects are at different depth in composite material – so using the proposed algorithm, it is possible to evaluate not only position, but the depth of the defects as well. Different depths of defects detected can be observed in the 3D C-scan, presented in Fig. 8.

After applying the developed post-processing algorithm defects were detected in different layers and in different positions – even between the pins. The signal processing technique proposed in this study was tested and experimentally verified using the immersion pulse-echo set-up. Such set-up was selected to demonstrate the principle of the proposed technique. However, the proposed technique is not limited to this particular arrangement and can be easily replaced in practical applications with measurements using water jet.

5. Conclusions

Additive manufacturing of a titanium adherend was combined with vacuum infusion of CFRP laminate to create a multi-material joint with both chemical and mechanical adhesion. This manufacturing method simultaneously creates the joint and the composite laminate, ensuring a high quality joint and laminate with few voids. However, during the manufacturing, due to poor surface preparation process, defects can occur in the dissimilar joint or in the composite itself, therefore non-destructive testing techniques, suitable for the inspection of dissimilar joints are needed.

It was shown that ultrasonic inspection from the composite side using high frequency focused ultrasonic transducer could be used for investigation of quality of dissimilar joints. In order to overcome the problems related to the rough surface and non-parallel layers a novel signal post-processing algorithm was developed. The presented results demonstrate that the proposed solution enables to detect the defects in the complex prefabricated titanium/carbon fibre composite joints and to estimate their position and depth. Hence, delaminations can be detected in different layers and in different positions – even close to the pins, as well as the missing pins.

Acknowledgment

The research leading to these results has received funding from the European Union Seventh Framework Programme under grant agreement n° 310498; project SAFEJOINT “Enhancing structural efficiency through novel dissimilar material joining techniques”.

References

[1] C. Cooper, G.J. Turvey, Effects of joint geometry and bolt torque on the structural performance of single bolt tension joints in pultruded GRP sheet material, Compos. Struct. 32 (1995) 217–226.
[2] K.I. Tserpes, G. Labeas, P. Papanikos, T. Kermanidis, Strength prediction of bolted joints in graphite/epoxy composite laminates, Compos. B Eng. 33 (2002) 521–529.
[3] F. Ascione, L. Feo, F. Maceri, On the pin-bearing failure load of GFRP bolted laminates: an experimental analysis on the influence of bolt diameter, Compos. B Eng. 41 (2010) 482–490.
[4] B. Egan, C.T. McCarthy, M.A. McCarthy, R.M. Frizzell, Stress analysis of single-bolt, single-lap, countersunk composite joints with variable bolt-hole clearance, Compos. Struct. 94 (2012) 1038–1051.
[5] Y. Zhai, D. Li, X. Li, L. Wang, Y. Yin, An experimental study on the effect of bolt-hole clearance and bolt torque on single-lap, countersunk composite joints, Compos. Struct. 127 (2015) 411–419.
[6] I.K. Giannopoulos, D. Doroni-Dawes, K.I. Kourousis, M. Yasaee, Effects of bolt torque tightening on the strength and fatigue life of airframe FRP laminate bolted joints, Compos. B Eng. 125 (2017) 19–26.
[7] U.A. Khashaba, H.E.M. Sallam, A.E. Al-Shorbagy, M.A. Seif, Effect of washer size and tightening torque on the performance of bolted joints in composite structures, Compos. Struct. 73 (2006) 310–317.
[8] G. Marannano, B. Zuccarello, Numerical experimental analysis of hybrid double lap aluminum-CFRP joints, Compos. B Eng. 71 (2015) 28–39.
[9] J. Ahamed, M. Joosten, P. Callus, S. John, C.H. Wang, Ply-interleaving technique for joining hybrid carbon/glass fibre composite materials, Compos. A Appl. Sci. Manuf. 84 (2016) 134–146.
[10] D.P. Graham, A. Rezai, D. Baker, P.A. Smith, J.F. Watts, The development and scalability of a high strength, damage tolerant, hybrid joining scheme for composite–metal structures, Compos. A Appl. Sci. Manuf. 64 (2014) 11–24.
[11] F.M.F. Ribeiro, R.D.S.G. Campilho, R.J.C. Carbas, L.F.M. da Silva, Strength and damage growth in composite bonded joints with defects, Compos. B Eng. 100 (2016) 91–100.
[12] D.N. Markatos, K.I. Tserpes, E. Rau, S. Markus, B. Ehrhart, S. Pantelakis, The effects of manufacturing-induced and in-service related bonding quality reduction on the mode-I fracture toughness of composite bonded joints for aeronautical use, Compos. B Eng. 45 (2013) 556–564.
[13] O. Ozdemir, N. Oztoprak, An investigation into the effects of fabric reinforcements in the bonding surface on failure response and transverse impact behavior of adhesively bonded dissimilar joints, Compos. B Eng. 126 (2017) 72–80.
[14] D. Yan, S.A. Neild, B.W. Drinkwater, Modelling and measurement of the nonlinear behaviour of kissing bonds in adhesive joints, NDT and E Int. 47 (2012) 18–25.
[15] C.V. Katsiropoulos, A.N. Chamos, K.I. Tserpes, S.G. Pantelakis, Fracture toughness and shear behavior of composite bonded joints based on a novel aerospace adhesive, Compos. B Eng. 43 (2012) 240–248.
[16] S. Ucsnik, M. Scheerer, S. Zaremba, D.H. Pahr, Experimental investigation of a novel hybrid metal–composite joining technology, Compos. A Appl. Sci. Manuf. 41 (2010) 369–374.
[17] R. Matsuzaki, M. Shibata, A. Todoroki, Improving performance of GFRP/aluminum single lap joints using bolted/co-cured hybrid method, Compos. A Appl. Sci. Manuf. 39 (2008) 154–163.
[18] B. Beylergil, Y. Cunedioglu, A. Aktas, Experimental and numerical analysis of single lap composite joints with inter-adherend fibers, Compos. B Eng. 42 (2011) 1885–1896.
[19] G. Marannano, B. Zuccarello, Static strength and fatigue life of optimized hybrid single lap aluminum–CFRP structural joints, J. Adhesion 1–28 (2017).
[20] G. Di Franco, B. Zuccarello, Analysis and optimization of hybrid double lap aluminum-GFRP joints, Compos. Struct. 116 (2014) 682–693.
[21] T.M. Koh, S. Feih, A.P. Mouritz, Experimental determination of the structural properties and strengthening mechanisms of z-pinned composite T-joints, Compos. Struct. 93 (2011) 2222–2230.
[22] M. Li, P. Chen, B. Kong, T. Peng, Z. Yao, X. Qiu, Influences of thickness ratios of flange and skin of composite T-joints on the reinforcement effect of Z-pin, Compos. B Eng. 97 (2016) 216–225.
[23] J.S. Boyce, G.A. Freitas, C.L. Magee, T.M. Fusco, J.J. Harris, Ultrasonic fastening system and method, WO 98/29243, 1998.
[24] L.W. Byrd, V. Birman, Effectiveness of z-pins in preventing delamination of co-cured composite joints on the example of a double cantilever test, Compos. B Eng. 37 (2006) 365–378.
[25] F. Pegorin, K. Pingkarawat, S. Daynes, A.P. Mouritz, Influence of z-pin length on the delamination fracture toughness and fatigue resistance of pinned composites, Compos. B Eng. 78 (2015) 298–307.
[26] D.P. Graham, A. Rezai, D. Baker, P.A. Smith, J.F. Watts, A hybrid joining scheme for high strength multi-material joints, 2011.
[27] S. Stelzer, S. Ucsnik, G. Pinter, Composite-composite joining with through the thickness reinforcements for enhanced damage tolerance, Mater. Sci. Forum 825–826 (2015) 883–890.
[28] S. Stelzer, S. Ucsnik, G. Pinter, Strength and damage tolerance of composite–composite joints with steel and titanium through the thickness reinforcements, Compos. A Appl. Sci. Manuf. 88 (2016) 39–47.
[29] P.N. Parkes, R. Butler, J. Meyer, A. de Oliveira, Static strength of metal-composite joints with penetrative reinforcement, Compos. Struct. 118 (2014) 250–256.
[30] P. Chang, A.P. Mouritz, B.N. Cox, Properties and failure mechanisms of z-pinned laminates in monotonic and cyclic tension, Compos. A Appl. Sci. Manuf. 37 (2006) 1501–1513.
[31] H. Ji, J. Kweon, J. Choi, Fatigue characteristics of stainless steel pin-reinforced composite hat joints, Compos. Struct. 108 (2014) 49–56.
[32] H. Son, Y. Park, J. Kweon, J. Choi, Fatigue behaviour of metal pin-reinforced composite single-lap joints in a hygrothermal environment, Compos. Struct. 108 (2014) 151–160.
[33] A.P. Mouritz, Review of z-pinned composite laminates, Compos. A Appl. Sci. Manuf. 38 (2007) 2383–2397.
[34] A.P. Mouritz, Delamination properties of z-pinned composites in hot–wet environment, Compos. A Appl. Sci. Manuf. 52 (2013) 134–142.
[35] I.K. Partridge, D.D.R. Cartié, Delamination resistant laminates by Z-Fiber® pinning: part I manufacture and fracture performance, Compos. A Appl. Sci. Manuf. 36 (2005) 55–64.
[36] F. Warzok, G. Allegri, M. Gude, S.R. Hallett, Experimental characterisation of

fatigue damage in single Z-pins, Part 2, Compos. Part A Appl. Sci. Manuf. 91 (2016) 461–471.
[37] A. Russo, B. Zuccarello, Toward a design method for metal-composite co-cured joints based on the G-SIFs, Compos. B Eng. 45 (2013) 631–643.
[38] S. Yang, L. Gu, R.F. Gibson, Nondestructive detection of weak joints in adhesively bonded composite structures, Compos. Struct. 51 (2001) 63–71.
[39] T.E.A. Ribeiro, R.D.S.G. Campilho, L.F.M. da Silva, L. Goglio, Damage analysis of composite–aluminium adhesively-bonded single-lap joints, Compos. Struct. 136 (2016) 25–33.
[40] S. Teixeira, de Freitas, J. Sinke, Failure analysis of adhesively-bonded skin-to-stiffener joints: metal–metal vs. composite–metal, Eng. Failure Anal. 56 (2015) 2–13.
[41] M.S. Islam, L. Tong, Influence of pinning on static strength of co-cured metal-GFRP hybrid single lap joints, Compos. A Appl. Sci. Manuf. 84 (2016) 196–208.
[42] S.M. Friedrich, A.S. Wu, E.T. Thostenson, T. Chou, Damage mode characterization of mechanically fastened composite joints using carbon nanotube networks, Compos. A Appl. Sci. Manuf. 42 (2011) 2003–2009.
[43] R.L. Vijaya Kumar, M.R. Bhat, C.R.L. Murthy, Some studies on evaluation of degradation in composite adhesive joints using ultrasonic techniques, Ultrasonics 53 (2013) 1150–1162.
[44] S.A. Titov, R.G. Maev, A.N. Bogachenkov, Pulse-echo NDT of adhesively bonded joints in automotive assemblies, Ultrasonics 48 (2008) 537–546.
[45] R. Tamborrino, D. Palumbo, U. Galietti, P. Aversa, S. Chiozzi, V.A.M. Luprano, Assessment of the effect of defects on mechanical properties of adhesive bonded joints by using non destructive methods, Compos. B Eng. 91 (2016) 337–345.
[46] D. Palumbo, R. Tamborrino, U. Galietti, P. Aversa, A. Tatì, V.A.M. Luprano, Ultrasonic analysis and lock-in thermography for debonding evaluation of composite adhesive joints, NDT E Int. 78 (2016) 1–9.
[47] W. Harizi, S. Chaki, G. Bourse, M. Ourak, Mechanical damage characterization of glass fiber-reinforced polymer laminates by ultrasonic maps, Compos. B Eng. 70 (2015) 131–137.
[48] J. Dong, B. Kim, A. Locquet, P. McKeon, N. Declercq, D.S. Citrin, Nondestructive evaluation of forced delamination in glass fiber-reinforced composites by terahertz and ultrasonic waves, Compos. B Eng. 79 (2015) 667–675.
[49] B. Ren, C.J. Lissenden, Ultrasonic guided wave inspection of adhesive bonds between composite laminates, Int. J. Adhes. Adhes. 45 (2013) 59–68.
[50] M.H. Sherafat, R. Guitel, N. Quaegebeur, P. Hubert, L. Lessard, P. Masson, Structural health monitoring of a composite skin-stringer assembly using within-the-bond strategy of guided wave propagation, Mater Des. 90 (2016) 787–794.
[51] C. Ramadas, J. Padiyar, K. Balasubramaniam, M. Joshi, C.V. Krishnamurthy, Lamb wave based ultrasonic imaging of interface delamination in a composite T-joint, NDT E Int. 44 (2011) 523–530.
[52] P. Ochôa, V. Infante, J.M. Silva, R.M. Groves, Detection of multiple low-energy impact damage in composite plates using Lamb wave techniques, Compos. B Eng. 80 (2015) 291–298.
[53] N. Mori, S. Biwa, Transmission of Lamb waves and resonance at an adhesive butt joint of plates, Ultrasonics 72 (2016) 80–88.
[54] C. Ramadas, K. Balasubramaniam, M. Joshi, C.V. Krishnamurthy, Interaction of Lamb mode (Ao) with structural discontinuity and generation of “Turning modes” in a T-joint, Ultrasonics 51 (2011) 586–595.
[55] R.S. Panda, P. Rajagopal, K. Balasubramaniam, Rapid guided wave inspection of complex stiffened composite structural components using non-contact air-coupled ultrasound, Compos. Struct. 206 (2018) 247–260.
[56] P. Pérès, D. Barnoncel, K. Balasubramaniam, M. Castaings, New experimental investigations of adhesive bonds with ultrasonic SH guided waves, ICCM International Conferences on Composite Materials, (2011).
[57] C.J. Brotherhood, B.W. Drinkwater, S. Dixon, The detectability of kissing bonds in adhesive joints using ultrasonic techniques, Ultrasonics 41 (2003) 521–529.
[58] G. Shui, Y. Wang, P. Huang, J. Qu, Nonlinear ultrasonic evaluation of the fatigue damage of adhesive joints, NDT E Int. 70 (2015) 9–15.
[59] C. Jeenjitkaew, F.J. Guild, The analysis of kissing bonds in adhesive joints, Int. J. Adhes. Adhes. 75 (2017) 101–107.
[60] M.F. Najib, A.S. Nobari, Kissing bond detection in structural adhesive joints using nonlinear dynamic characteristics, Int. J. Adhes. Adhes. 63 (2015) 46–56.
[61] M. Rothenfusser, M. Mayr, J. Baumann, Acoustic nonlinearities in adhesive joints, Ultrasonics 38 (2000) 322–326.
[62] B. Zhang, G. Allegri, M. Yasaee, S.R. Hallett, Micro-mechanical finite element analysis of Z-pins under mixed-mode loading, Compos. A Appl. Sci. Manuf. 78 (2015) 424–435.
[63] A.P. Mouritz, Compression properties of z-pinned composite laminates, Composites Sci. Technol. 67 (2007) 3110–3120.
[64] F. Bianchi, T.M. Koh, X. Zhang, I.K. Partridge, A.P. Mouritz, Finite element modelling of z-pinned composite T-joints, Compos. Sci. Technol. 73 (2012) 48–56.
[65] T.M. Koh, S. Feih, A.P. Mouritz, Strengthening mechanics of thin and thick composite T-joints reinforced with z-pins, Compos. A Appl. Sci. Manuf. 43 (2012) 1308–1317.
[66] K. Milne, P. Cawley, P.B. Nagy, D.C. Wright, A. Dunhill, Ultrasonic non-destructive evaluation of titanium diffusion bonds, J. Nondestr. Eval. 30 (2011) 225–236.